

Estimation of local and nonlocal contributions to the current-induced magnetization switching

T. Yang,^{1,*} A. Hirohata,¹ T. Kimura,^{1,2} and Y. Otani^{1,2}

¹Frontier Research System, RIKEN, 2-1 Hirosawa, Wako, Saitama 351-0198, Japan

²Institute for Solid State Physics, University of Tokyo, Kashiwa, Chiba 277-8581, Japan

(Received 31 July 2006; revised manuscript received 28 August 2006; published 4 October 2006)

With the experimental results obtained with a special nanopillar structure and the calculations based on the one-dimensional diffusion equations, the respective contributions to the spin torque from spin accumulation and local spin current are quantitatively deduced. The results for a typical nanopillar structure show that the spin accumulation contributes to about 90% of the necessary torque for the antiparallel to parallel switching, while the parallel to antiparallel switching is totally dominated by the local spin current. Both the variations in spin accumulation and local spin current should be considered in any effort to reduce the critical switching current density. However it seems more effective to increase the local spin current in most cases.

DOI: [10.1103/PhysRevB.74.153301](https://doi.org/10.1103/PhysRevB.74.153301)

PACS number(s): 73.63.-b, 85.75.Bb, 72.25.Ba

As a new approach to switch a nanomagnet, the current-induced magnetization switching (CIMS) (Refs. 1 and 2) is interesting not only for fundamental research, but also for a practical purpose. Therefore, it has been extensively investigated³⁻⁶ with a ferromagnet (FM)/nonmagnet (NM)/FM nanopillar structure. CIMS is caused by the spin-transfer effect.¹ When a spin current enters a magnet, the transverse component of the spin angular momentum is absorbed both at the interface^{1,7} and inside the magnet,^{7,8} exerting a spin torque on the local magnetic moment.

Remarkable is that the origin of the spin current is still controversial. Usually, a spin-polarized local electrical current J_e carries a spin current J_S , called local spin current.⁹ On the other hand, the spin accumulation $\Delta\mu$ is also reported to produce a nonlocal spin current.^{9,10} While the local spin current is a fraction of J_e , the nonlocal spin current is proportional to the magnitude of $\Delta\mu$. The ratio of the local and the nonlocal contributions to the spin torque is theoretically estimated to be the ratio of electron mean free path and spin diffusion length, i.e., about 0.01–0.1. Therefore, the main contribution to the CIMS should be from the spin accumulation.^{9,10}

Some experimental results support the above theoretical conclusion.¹¹ However, there are also evidences suggesting that the main contribution is from the local spin current J_S .^{12,13} To explain these contradictory results, it is necessary to evaluate the respective contributions of the local spin current and the spin accumulation quantitatively. Such data are very important not only for further understanding the mechanism, but also for deciding the strategy to reduce the switching current density, which is critical for practical application. However, experimental efforts are still absent on this issue.

In principle, the local and the nonlocal contributions can be deduced by comparing the critical switching current density J_C as well as the local spin current and the spin accumulation between two different nanopillars. Usually, the top FM layer in the nanopillar is a very thin nanomagnet switchable by the current while the bottom FM layer is thick and magnetically fixed during CIMS. When there is a slight deviation from the collinear magnetic configuration of the two FM layers, the top nanomagnet absorbs the transverse component of the spin current and is thus applied the spin torque. For unit cross-sectional area, if we denote the contributions to

the spin torque from unit spin accumulation and unit local spin current density as x and y respectively, the critical spin torque to switch the nanopillar is written as $\Gamma_C = J_C S (\delta\mu x + p y)$, where S is the cross-sectional area, p and $\delta\mu$ are respectively the local spin current density and the spin accumulation produced by unit electrical current density. When the switched nanomagnets in both nanopillars are identical, we have

$$J_{C1}/J_{C2} = (\delta\mu_2 x + p_2 y) / (\delta\mu_1 x + p_1 y). \quad (1)$$

Here, the subscripts 1 and 2 denote the two samples respectively. According to the ratio of x and y obtained from Eq. (1), we can estimate the local and the nonlocal contributions, i.e., the contributions from the local spin current and the spin accumulation respectively.

However, the comparison of the critical switching current density between two nanopillars is not always reliable, especially for quantitative purpose. Except for the uncertainty when measuring the cross-sectional area of a nanopillar as small as ~ 100 nm, the sample-to-sample variation in the thermal stability also affects the critical switching current density.¹⁴⁻¹⁶

In addition, it should be pointed out that when the spin-polarized current traverses a nanomagnet, the spin torque also depends on the angle θ between the spin-polarization direction of the current and the majority spin direction in the nanomagnet.^{1,17} Thus, for collinear configuration, we denote y as y_0 or y_π when θ is 0 or π , respectively. Therefore, we need at least two equations such as Eq. (1) to deduce the respective contributions from the local spin current and the spin accumulation.

In this work, we fabricated a nanopillar as shown in Fig. 1. The magnetic configuration of the three Co layers decides the spin accumulation and the local spin current inside the structure. If we study the switching of Co3 layer in varied magnetic configurations, there is no size difference at all. If the measuring conditions are strictly the same, the effect of the thermal fluctuation can also be ruled out.^{15,16} Comparing the critical switching currents of Co3 layer in varied magnetic configurations and utilizing the calculated spin accumulations as well as the calculated local spin current densities,

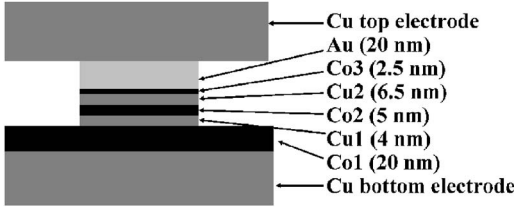


FIG. 1. Schematic structure of the studied nanopillar.

we can deduce the respective contributions from the local spin current and the spin accumulation.

When there is only a slight deviation from the collinear configuration, either the spin current or the spin accumulation can be regarded as longitudinal. Hence, both the spin accumulation and the local spin current in this paper are the longitudinal ones.

The layer thicknesses of the nanopillar are carefully chosen to optimize the coercivity for each Co layer and the dipolar coupling between Co layers, so that various magnetic configurations can be realized and only the Co3 layer is switched during the CIMS measurement.

The transport properties are measured with lock-in technique at room temperature when applying an external field along the easy axis of the nanopillar. The CIMS measurement is carried out with a pulsed current I_{pu} . The pulse width is fixed at 0.1 s. The electrical current flowing from the bottom to the top is defined as positive.

Figures 2(a) and 2(b) are the full and minor magnetoresistance (MR) loops, respectively. All four possible magnetic states or configurations appear in the MR loops, characterized and labeled as A, B, C, and D, respectively according to the different coercive fields of the Co layers. The dipolar coupling field exerted on Co3 layer is determined from the minor loop to be 190 Oe.

To measure the critical switching current densities of Co3 layer, B to D, C to A, and A to C switches are studied. Each initial state has its own spin accumulation and local spin current density at the Cu2/Co3 interface, and hence its own critical switching current density for Co3 layer.

A negative pulsed current is applied to switch the B or C state. For both B to D and C to A switches, the differential resistance dV/dI is measured after each pulse and plotted in Fig. 3(a) as the function of I_{pu} . For state B, the measurement is carried out under an external field of 60 Oe. Including the dipolar coupling field, the effective field applied on Co3

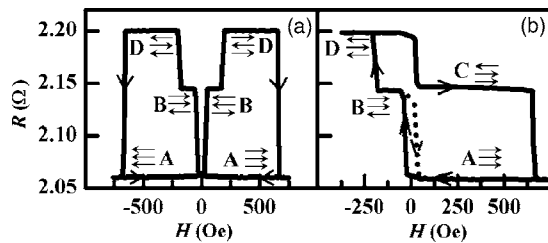


FIG. 2. (a) Full and (b) minor MR loops. The three arrows for each state represent the magnetizations of Co1, Co2, and Co3 layers, respectively. There are two minor loops in (b) indicated with solid and dotted lines, respectively.

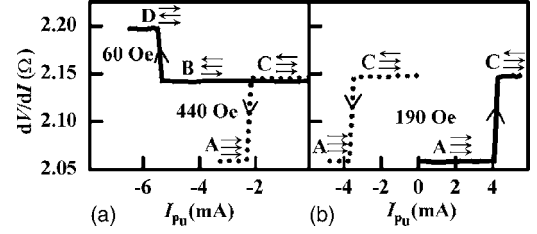


FIG. 3. Current-induced magnetization switching of Co3 layer. (a) B to D and C to A switches, as well as (b) C to A and A to C switches. The magnetic fields applied during measurements are indicated in the figures.

layer is 250 Oe. To keep the same measuring conditions, an external field of 440 Oe is applied for state C to ensure the same effective field and thus the same thermal stability of Co3 layer.^{15,16} The measured critical switching currents are -5.5 mA and -2.3 mA for B to D and C to A switches, respectively. Substituting the critical switching currents into Eq. (1), we obtain

$$5.5/2.3 = (\delta\mu_{Cx} + p_{Cy}) / (\delta\mu_{Bx} + p_{By}). \quad (2)$$

With an external field of 190 Oe, the critical switching current from C to A becomes -3.7 mA, while the transition from A to C occurs at $+4.3$ mA, as shown in Fig. 3(b). For both switches, the effective fields applied on Co3 layer are 0 Oe. Hence the second equation can be established as

$$4.3/3.7 = (\delta\mu_{Cx} + p_{Cy}) / (\delta\mu_{Ax} + p_{Ay}). \quad (3)$$

Values of p and $\delta\mu$ in Eqs. (2) and (3) are calculated based on the one-dimensional diffusion equations^{18,19}

$$J_{\uparrow,\downarrow} = (\sigma_{\uparrow,\downarrow}/e)(\partial\mu_{\uparrow,\downarrow}/\partial x), \Delta\mu/\lambda^2 = \partial^2\Delta\mu/\partial x^2, \quad (4)$$

where λ , μ , σ , and e are respectively the spin-diffusion length, the electrochemical potential, the electrical conductivity, and the electronic charge. Spin-up (\uparrow) is the direction of the majority spin in Co1 layer.

Taking into account the interfacial spin-dependent scattering but neglecting the very small interfacial spin flip,^{20,21} we have two equations at each interface. By solving all the equations, we can obtain both spin accumulation and local spin current in each layer.

Equation (4) is for one-dimensional structure. It requires the cross-sectional area of the whole nanopillar, including the electrodes, to be constant. But in the real structure the electrodes are extended. The size of the electrode has been reported to influence both spin accumulation and local spin current significantly,^{22,23} omitted in most of the theoretical works. After entering the electrode, the current flows not only vertically but also horizontally. Therefore the current flow is not one-dimensional and the cross-sectional area is greatly increased. The electrode thus provides increased volume for spin relaxation. As the results of the enhanced spin relaxation, the local spin current is increased while the spin accumulation is suppressed inside the nanopillar. The enhanced spin relaxation can also be explained with the spin

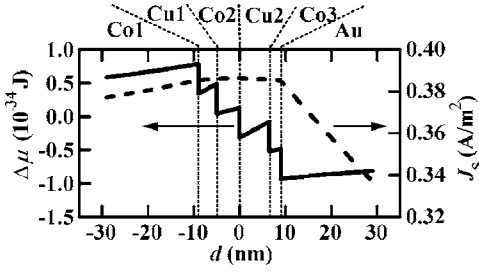


FIG. 4. Calculated spin accumulation (solid line) and local spin current (dashed line) curves for A state with a 1 A/m^2 electrical current density. Positive value means the spin-up direction. d is the distance to the Co2/Cu2 interface in the nanopillar.

resistance $R_S = \lambda / [S\sigma(1 - \alpha^2)]$, where α is the spin asymmetry. The increased S reduces the spin resistance, therefore enhances the spin relaxation.

To evaluate the size effect of the electrode, Berger has developed a set of spin-diffusion equations especially for the extended electrode.²²

In our calculations, we still assume the constant cross section. Instead, an effective conductivity for the electrode is used to simulate the size effect. This is because both increases in the cross-sectional area and the conductivity reduce the spin resistance and hence enhance the spin relaxation. To find the suitable effective conductivity for the electrodes, we calculated the spin accumulation and the local spin current in the multilayered structure described in Berger's paper²² using the one-dimensional method and various effective conductivity values. In all our calculations, we use the same set of materials parameters²⁴ as that used in Berger's calculation. When the ratio between the effective and the original conductivities is 6, we can reproduce Berger's results obtained with the special diffusion equations for the extended electrode.²²

Therefore, the size effect of the extended electrode is equivalent to increasing the conductivity by a factor of 6. We use this factor in the following calculations.

Compared with the Cu electrode, the size effect of the unpatterned Co1 layer is small. Because of the large difference in the conductivity between Co and Cu, almost all the horizontal current flows in the Cu bottom electrode. Thus the electrical current flows in the Co1 layer still almost vertically before entering the Cu bottom electrode. The effective conductivity factor for Co1 layer is chosen in such a way that the calculated ΔR values are closest to the measured ones shown in Fig. 2. The best effective conductivity factor is 1.4 for Co1 layer.

Figure 4 shows the calculated spin accumulation and local spin current curves for state A. The electrical current density is assumed to be 1 A/m^2 . The calculated values of $\delta\mu$ and p are listed in Table I for A, B, and C states. We choose the values at the Cu2/Co3 interface in the Cu2 layer rather than the Co3 layer to include the interfacial absorption. Positive direction means spin-up direction.

According to the sign of p , y is determined to be y_0 , y_0 , and y_π for states A, B, and C, respectively. Substituting the calculated results into Eqs. (2) and (3), we obtain

$$y_0/x = 9.0 \times 10^{-34} \text{ Jm}^2/\text{A}, \quad y_\pi/x = 3.9 \times 10^{-34} \text{ Jm}^2/\text{A}. \quad (5)$$

TABLE I. Calculation results for the nanopillar shown in Fig. 1.

Configuration	A	B	C
$\delta\mu$ ($10^{-34} \text{ J m}^2/\text{A}$)	-0.07	2.03	3.38
p	0.39	-0.03	0.19

With Eq. (23) in Ref. 2, it is roughly estimated that 1 A/m^2 local spin current density is theoretically equivalent to $2.0 \times 10^{-34} \text{ J}$ spin accumulation, in term of their contributions to the spin torque. Our results given by Eq. (5) suggest that 1 A/m^2 local spin current density is equivalent to $6.5 \times 10^{-34} \text{ J}$ spin accumulation in average.

With results given by Eq. (5), we investigate a typical nanopillar structure, Cu electrode/Co1(15 nm)/Cu(6 nm)/Co2(2.5 nm)/Au(10 nm)/Cu electrode. We consider two cases, i.e., constant cross section and extended electrode. Co1 layer is also extended for the latter.

Table II lists the calculated $\delta\mu$ and p for both cases. Based on these data and the results given by Eq. (5), the respective contributions to the spin torque from the spin accumulation and the local spin current, as well as the torque produced by unit electrical current density are deduced and also listed in the table.

It is shown that regardless of the electrode size, the spin accumulation contributes to about 90% of the spin torque necessary for antiparallel (AP) to parallel (P) switching while the P to AP transition is completely caused by the local spin current. Thus the two opposite switches have different mechanisms. The ratio 0.01–0.1 is the theoretical expectation given without considering the electrode size.^{9,10} When the electrode size is considered, it is reported that the local and nonlocal contributions become comparable for the P to AP switching.⁹

The main difference between the constant cross section case and the extended electrode case is that the torque produced by unit electrical current density in the P state is much larger for the latter than that for the former. This is caused by the significantly enhanced local spin current.

TABLE II. Results for the typical nanopillar. T : Spin torque produced by unit electrical current. C_{J_s} : Local spin current contribution to the spin torque. $C_{\Delta\mu}$: Spin accumulation contribution to the spin torque.

	Constant cross section		Extended electrode	
	P	AP	P	AP
p	0.20	0.07	0.34	0.09
$\delta\mu(10^{-34})$	0.08	2.96	0.05	2.77
T	1.72x	3.23x	3.01x	3.12x
C_{J_s}	100%	8%	100%	11%
$C_{\Delta\mu}$... ^a	92%	... ^a	89%
$C_{J_s}/C_{\Delta\mu}$ (Theor.)	0.01–0.1 ^b			

^aThe positive spin accumulation hinders the P to AP switching. Therefore its contribution is not considered.

^bReferences 9 and 10.

Interesting is that the AP state is only slightly affected by the electrode size. In the AP configuration the local spin current flow is greatly reduced, due to the nonequilibrium spin accumulation in the Cu spacer between the two antiparallel Co layers. The accumulated spin is hardly affected by any change occurring outside the Co1/Cu/Co2 trilayer. As a result, for the AP state, the extended electrode only causes a small reduction of 4% in the spin torque per unit electrical current density. For the P state, both the local spin current density and the spin accumulation are significantly affected by the electrode size. The spin torque per unit electrical current density is increased by 75% when the electrode becomes extended. Thus the total critical switching current density is reduced by the increased electrode size, in agreement with previous experimental results on the effect of the electrode.²⁵

Since both spin accumulation and local spin current contribute to the CIMS, any strategy to reduce the switching current density should consider the variations in both the spin accumulation and the local spin current. The idea way is to increase the spin accumulation and the local spin current

simultaneously, e.g., using materials with high spin asymmetry.²⁶ However, since the AP state is difficult to be affected, it may be more effective to reduce the P to AP critical switching current density by improving the local spin current, e.g., through enhancing the spin relaxation in the capping layer or the electrode.^{12,13} In some special cases, such as the antisymmetrical structure,^{11,27,28} where the spin accumulation can be greatly improved, the critical switching current density can also be reduced.

In conclusion, we have deduced a ratio of the contributions to the spin torque from unit spin accumulation and unit local spin current density respectively. For a typical nanopillar, it is found that the P to AP switching is dominated by the local spin current, while the AP to P switching is more non-local, i.e., dominated by the spin accumulation.

We are grateful to K. Tsukagoshi and the Nanoscience Development and Support Team of RIKEN for their great support.

*Corresponding author. Email address: tyang@riken.jp

¹J. C. Slonczewski, *J. Magn. Magn. Mater.* **159**, L1 (1996).

²L. Berger, *Phys. Rev. B* **54**, 9353 (1996).

³M. Tsoi, A. G. M. Jansen, J. Bass, W.-C. Chiang, M. Seck, V. Tsoi, and P. Wyder, *Phys. Rev. Lett.* **80**, 4281 (1998).

⁴J. A. Katine, F. J. Albert, R. A. Buhrman, E. B. Myers, and D. C. Ralph, *Phys. Rev. Lett.* **84**, 3149 (2000).

⁵J. Grollier, V. Cros, A. Hamzic, J. M. George, H. Jaffrès, A. Fert, G. Faini, J. Ben Youssef, and H. Legall, *Appl. Phys. Lett.* **78**, 3663 (2001).

⁶J. Z. Sun, D. J. Monsma, D. W. Abraham, M. J. Rooks, and R. H. Koch, *Appl. Phys. Lett.* **81**, 2202 (2002).

⁷M. D. Stiles and A. Zangwill, *Phys. Rev. B* **66**, 014407 (2002).

⁸S. Zhang, P. M. Levy, and A. Fert, *Phys. Rev. Lett.* **88**, 236601 (2002).

⁹L. Berger, *J. Appl. Phys.* **89**, 5521 (2001).

¹⁰A. Fert, V. Cros, J.-M. George, J. Grollier, H. Jaffrès, A. Hamzic, A. Vaurès, G. Faini, J. Ben Youssef, and H. Le Gall, *J. Magn. Magn. Mater.* **272-276**, 1706 (2004).

¹¹Y. Jiang, G. H. Yu, Y. B. Wang, J. Teng, T. Ochiai, N. Tezuka, and K. Inomata, *Appl. Phys. Lett.* **86**, 192515 (2005).

¹²S. Urazhdin, N. O. Birge, W. P. Pratt, Jr., and J. Bass, *Appl. Phys. Lett.* **84**, 1516 (2004).

¹³T. Yang, A. Hirohata, T. Kimura, and Y. Otani, *J. Appl. Phys.* **99**, 073708 (2006).

¹⁴F. J. Albert, N. C. Emley, E. B. Myers, D. C. Ralph, and R. A. Buhrman, *Phys. Rev. Lett.* **89**, 226802 (2002).

¹⁵R. H. Koch, J. A. Katine, and J. Z. Sun, *Phys. Rev. Lett.* **92**, 088302 (2004).

¹⁶Z. Li and S. Zhang, *Phys. Rev. B* **69**, 134416 (2004).

¹⁷J. Z. Sun, *IBM J. Res. Dev.* **50**, 81 (2006).

¹⁸P. C. van Son, H. van Kempen, and P. Wyder, *Phys. Rev. Lett.* **58**, 2271 (1987).

¹⁹T. Valet and A. Fert, *Phys. Rev. B* **48**, 7099 (1993).

²⁰H. Kurt, Wen-C. Chiang, C. Ritz, K. Eid, W. P. Pratt, Jr., and J. Bass, *J. Appl. Phys.* **93**, 7918 (2003).

²¹WanJun Park, David V. Baxter, S. Steenwyk, I. Moraru, W. P. Pratt, Jr., and J. Bass, *Phys. Rev. B* **62**, 1178 (2000).

²²L. Berger, *J. Magn. Magn. Mater.* **278**, 185 (2004).

²³J. Hamrle, T. Kimura, T. Yang, and Y. Otani, *Phys. Rev. B* **71**, 094434 (2005).

²⁴L. Piroux, S. Dubois, A. Fert, and L. Belliard, *Eur. Phys. J. B* **4**, 413 (1998).

²⁵T. Yang, J. Hamrle, T. Kimura and Y. Otani, *Appl. Phys. Lett.* **87**, 162502 (2005).

²⁶Y. Jiang, S. Abe, T. Ochiai, T. Nozaki, A. Hirohata, N. Tezuka, and K. Inomata, *Phys. Rev. Lett.* **92**, 167204 (2004).

²⁷L. Berger, *J. Appl. Phys.* **93**, 7693 (2001).

²⁸S. Nakamura, S. Haneda, and H. Morise, *J. Appl. Phys.* **45**, 3846 (2006).